Proceedings of the 4th International Conference on Functional Materials and Civil Engineering
DOI: 10.54254/2755-2721/2026.36617

Photocatalytic Integrated CO_2 Capture and Conversion to Methanol Using Modified MXene Quantum Dots

Yixiao Qiu

School of Mechanical Engineering, Zhejiang University of Technology, Hangzhou, China
2752646953@qq.com

Abstract. With atmospheric CO_2 concentrations exceeding 420 ppm worldwide, the global climate crisis has intensified, establishing direct air capture and utilization (DACU) as a critical pathway toward achieving the "dual carbon" goals. However, the elevated energy demand and CO_2 inertness of conventional carbon capture technologies severely limit their practical applications. In response to these limitations,, MXene quantum dots (MQDs) have emerged as promising candidates for photocatalytic DAC-CO_2 reduction, owing to their quantum confinement effects, tunable bandgaps, and rich surface chemistry. Therefore, this study establishes a framework of "theory-design-mechanism" and proposes MQD-based photocatalytic systems through N/S co-doping, g-C_3N_4 heterojunctions, and Cu single-atom engineering. Through literature synthesis and theoretical analysis, this study examines the effects of band structure engineering on charge separation, the influence of surface Lewis basic sites in CO_2 activation, and the potential catalytic mechanism of Cu sites for CO intermediate hydrogenation. The analysis shows that this design is theoretically conducive to addressing the challenges of adsorption/activation and directed multi-electron reduction conversion of CO_2 at ultra-low concentrations, and provides reference insights for the design of solar-driven negative-carbon conversion materials.

Keywords: MXene Quantum Dots, Photocatalysis, Direct Air Capture, CO_2 Reduction, Methanol Synthesis

1. Introduction

In the face of intensifying global warming and limited mitigation efforts, reliance solely on energy transitions is insufficient to achieve the Paris Agreement's 1.5 °C target. Direct air capture (DAC) has been recognized as a critical negative-emission technology pathway owing to its capability to directly remove CO_2 from the atmosphere [1-3]. However, the low partial pressure of CO_2 (~40 Pa) constrains its capture efficiency, and existing DAC processes based on chemical amine absorption or temperature/vacuum swing adsorption suffer from high energy consumption (~8–12 GJ·t^{-1} CO_2) and material deactivation issues [4, 5]. To reduce energy consumption and achieve high-value CO_2 conversion, coupling DAC with solar-driven photocatalytic CO_2 reduction (CO_2RR) to produce liquid fuels has been proposed. In particular, MXene quantum dots (MQDs), as zero-dimensional materials derived from MXene, possess high electrical conductivity, quantum confinement effects, and abundant edge active sites, thereby enabling the regulation of electron transfer processes in

© 2026 The Authors. This is an open access article distributed under the terms of the Creative Commons Attribution License 4.0 (https://creativecommons.org/licenses/by/4.0/).

DOI: 10.54254/2755-2721/2026.36617

photocatalytic CO_2RR [6, 7]. Among them, $Ti_3C_2T_x$-derived MQDs feature surface –O, –OH, and –F functional groups that can serve as CO_2 adsorption sites. However, challenges remain, including limited visible-light absorption, rapid carrier recombination, and poor selectivity for multi-electron reduction. Previous studies have modulated the band structure and interfacial charge transport of MQDs via heteroatom doping, g-C_3N_4 heterostructure construction, and single-atom modification, influencing CO_2 adsorption and the pathways of key intermediates such as *CO. Nevertheless, under low-concentration CO_2 conditions, the coupling mechanism between adsorption/activation capability and the selectivity toward six-electron reduction (methanol generation) remains unclear [8]. Based on literature synthesis and theoretical analysis, this review surveys the recent progress in photocatalytic CO_2 conversion using modified MXene quantum dots under DAC conditions. The focus is placed on elucidating the regulatory roles of heteroatom doping, g-C_3N_4 heterostructures, and single-atom modification on band structure, interfacial charge transport, and surface electronic properties, as well as their effect on CO_2 adsorption/activation and the *CO intermediate conversion pathways.

2. Fundamental principles and reaction mechanisms of photocatalytic CO_2 conversion

2.1. Generation of photogenerated charge carriers and reaction mechanisms

The photocatalytic process is initiated by the absorption of photons by the semiconductor, which subsequently triggers interband electron transitions. Specifically, when the incident photon energy matches or exceeds the bandgap energy (E_g), valence band electrons are excited to the conduction band, thus leading to the formation of electron-hole pairs, as shown in Figure 1. The photogenerated carriers migrate toward the catalyst surface under the driving forces of the built-in electric field and concentration gradients, where they participate in CO_2 reduction and water oxidation reactions. But bulk defects, lattice disorder, and interfacial defects can promote electron-hole recombination, thus lowering carrier utilization efficiency. As such, carrier separation and interfacial migration strongly influence photocatalytic CO_2 reduction performance.

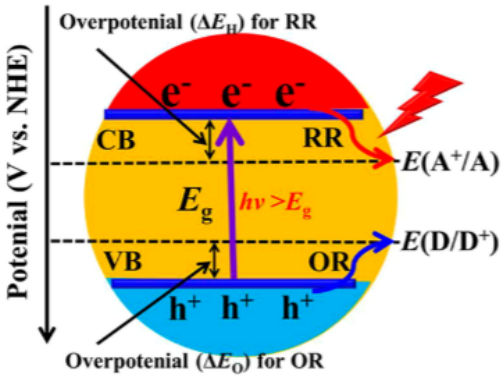

Figure 1. Band structure mechanism of semiconductor photocatalysis

The photogenerated carriers exhibit different behaviors in various semiconductors. In inorganic semiconductors, free electron-hole pairs are typically generated, while polymeric semiconductors such as g-C_3N_4 form Frenkel excitons due to their low dielectric constants. These excitons possess binding energies of approximately 0.3-0.6 eV and require interfacial electric fields or energy-level offsets to facilitate exciton dissociation [9, 10]. In MQD/g-C_3N_4 heterojunction systems, interfacial

DOI: 10.54254/2755-2721/2026.36617

band matching can facilitate exciton separation and achieve spatial regulation of carrier distribution via the S-scheme heterojunction mechanism: electrons in the conduction band of g-C_3N_4 recombine with holes in the valence band of MQDs at the interface, while the MQD side retains electrons with strong reducing capability and the g-C_3N_4 side retains holes with strong oxidizing capability, thus simultaneously maintaining potent reduction and oxidation capacities.

2.2. CO_2 adsorption/activation and multi-electron reduction processes

Under direct air capture (DAC) conditions, the low concentration of CO_2 (approximately 420 ppm) renders adsorption enrichment and molecular activation critical steps that limit reduction efficiency. Physical adsorption mainly relies on weak van der Waals interactions, making effective enrichment difficult to achieve. In contrast, electron-rich surface sites can chemically adsorb CO_2, inducing molecular bending and the formation of activated intermediates like CO_2•⁻, facilitating subsequent electron transfer and bond activation processes [11, 12].

Following CO_2 activation, the reduction process primarily involves multielectron-proton coupled pathways. The one-electron reduction pathway, which generates CO_2•⁻, requires a highly negative potential of approximately −1.9 V and involves a large energy barrier, making it unfavorable under conventional photocatalytic conditions. In contrast, multielectron reduction pathways require lower potentials. For example, the standard potential for CO_2 reduction to CH_3OH ($CO_2 + 6H^+ + 6e^- \rightarrow CH_3OH + H_2O$) is −0.38 V, which shifts to around −0.79 V at pH 7, indicating a reduced driving force requirement. Therefore, CO_2 reduction mainly follows a stepwise hydrogenation route, where CPET stabilizes intermediates and avoids high-energy single-electron steps [13]. As illustrated in Figure 2, CO_2 conversion involves two main stages: adsorption-induced activation and sequential reduction. Notably, CO_2 activation and interfacial charge transfer affect conversion efficiency under dilute conditions.

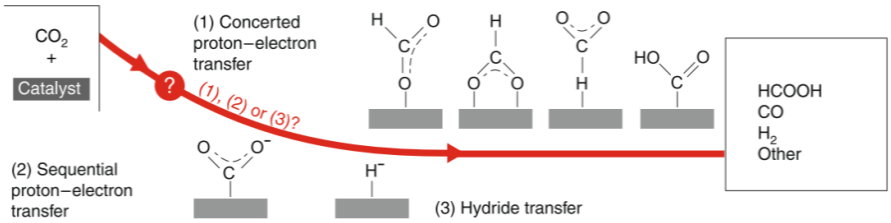

Figure 2. CO_2 adsorption/activation and conversion routes

2.3. Structural properties and size effects of quantum dots

When semiconductor dimensions shrink below the exciton Bohr radius, quantum confinement alters electronic structures, resulting in discrete energy levels, enlarged bandgaps, blue-shifted absorption edges, and tunable band positions [14]. This size-dependent effect alters the light absorption range and conduction band reduction ability, affecting the energy matching in CO_2 reduction processes.

From a charge dynamics perspective, size reduction shortens carrier diffusion distances, allowing electrons and holes to reach the surface before bulk recombination, improving the effective carrier utilization efficiency. Concurrently, the specific surface area increases rapidly with decreasing size, with surface atoms constituting more than 50% of the total, leading to enhanced uncoordinated site density and improved CO_2 adsorption and initial capture probability under low partial pressure (~420 ppm) conditions. Therefore, the size effect of quantum dots does not act independently on the band structure, charge transport, and surface properties; rather, through the dominant mechanism of

DOI: 10.54254/2755-2721/2026.36617

electronic structure reconstruction, it regulates band positions, carrier migration lengths, and surface active site density, collectively determining the overall reaction performance in DAC photocatalytic systems. In MXene quantum dot systems, this effect is further amplified through interfacial charge redistribution.

3. MXene quantum dot systems and structural engineering strategies

3.1. Performance comparison of mainstream quantum dot materials

The performance differences among quantum dots in photocatalytic CO_2 conversion primarily stem from their band structures, surface properties, and charge transport. In particular, carbon quantum dots (CQDs) exhibit good photostability and tunable electronic structures; however, their reduction ability and CO_2 activation are limited by surface groups and electronic structures. In contrast, CdS QDs demonstrate strong visible-light responsiveness but suffer from photocorrosion and Cd-related environmental concerns [15].

In comparison, $Ti_3C_2T_x$ MXene quantum dots (MQDs) combine high electrical conductivity with abundant surface groups (–O, –OH, –F), enabling enhanced electron transport and strengthened CO_2 adsorption/activation. Studies have shown that edge Ti sites can coordinate with CO_2, inducing molecular configuration changes and facilitating subsequent reduction reactions [16]. A comparison of key performance parameters among different quantum dot materials is presented in Table 1.

Table 1. Performance comparison of mainstream quantum dot materials

Parameter	CQDs	CdS QDs	MXene QDs ($Ti_3C_2T_x$)
Bandgap (eV) [6, 15]	2.0–4.0	~2.4	1.5–3.0 (size-tunable)
CO_2 adsorption capacity ($mmol \cdot g^{-1}$) [6, 15, 16]	0.2–0.5	0.1–0.3	0.5–1.2
Carrier lifetime [6, 15, 17]	1–5 ns	10–100 ns	0.5–4 ns (modification-enhanced)
Electrical conductivity ($S \cdot cm^{-1}$) [6, 15]	10^{-2}–10^{0}	10^{-6}–10^{-4}	~10^{4}
Photostability [15]	Good	Poor (photocorrosion)	Good
Toxicity [15]	Low	High (Cd-based)	Low

3.2. Structural regulation strategies for MXene quantum dots

The difficulty in single modification strategies lies in their inability to simultaneously optimize light harvesting, charge separation, and surface reactions in DAC photocatalysis, as band, interface, and surface regulation address distinct functions.

Band regulation can extend the light response range but may introduce defect recombination centers. Meanwhile, interface engineering promotes directional charge transfer but provides limited control over surface active sites. In addition, surface modification facilitates CO_2 adsorption and intermediate stabilization but relies on efficient carrier supply. Thus, MQD modification strategies are shifting from single regulation toward synergistic multi-strategy integration, constructing a continuous "light harvesting-charge separation-surface reaction" pathway to boost overall catalytic performance, as shown in Figure 3.

DOI: 10.54254/2755-2721/2026.36617

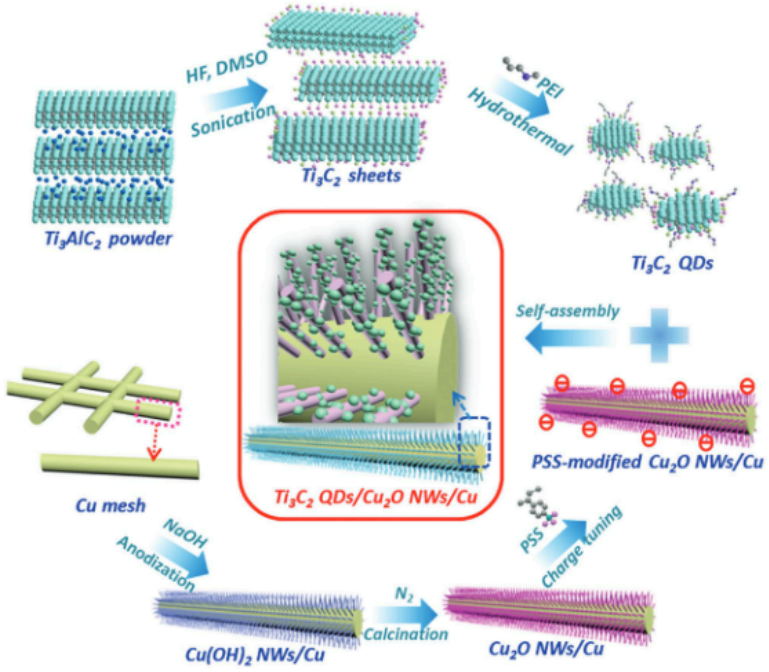

Figure 3. Triple synergistic regulation strategies (doping/heterojunction/single-atom modification)

Regarding band regulation, N and S co-doping can modify the electronic structure of MQDs by introducing dopant states, influencing the bandgap and visible-light response while adjusting the valence band position and redox capability [18]. Specifically, N doping may regulate the electronic states near the Fermi level via orbital hybridization, while S doping mainly affects the valence band structure. Their synergistic effects are expected to optimize light absorption and carrier migration. And theoretical calculations predict that appropriate N doping can reduce the bandgap of $Ti_3C_2T_x$MQDs from approximately 2.8 eV to 2.1 eV, consistent with the absorption-edge red shift reported in previous studies. Heterostructure construction further regulates the band alignment and interfacial charge transfer of MQDs. The g-C_3N_4/MQDs S-scheme heterojunction promotes photogenerated carrier migration through interfacial band coupling, as shown in Figure 4.

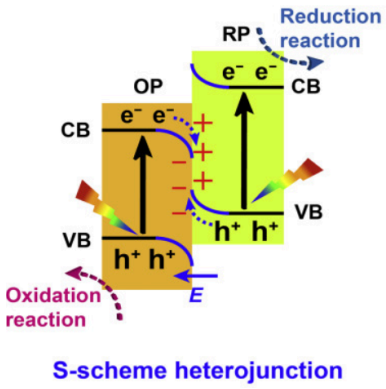

Figure 4. Band structure of the g-C_3N_4/MQDs S-scheme heterojunction

For interface regulation, the g-C_3N_4/MQDs heterostructure facilitates spatial charge separation via band alignment and an internal electric field, forming an S-scheme charge transfer pathway, as

DOI: 10.54254/2755-2721/2026.36617

shown in Figure 5 [10]. This structure selectively retains electrons with strong reduction ability and holes with strong oxidation ability, improving charge utilization efficiency while maintaining the redox capability required for CO_2 reduction and water oxidation.

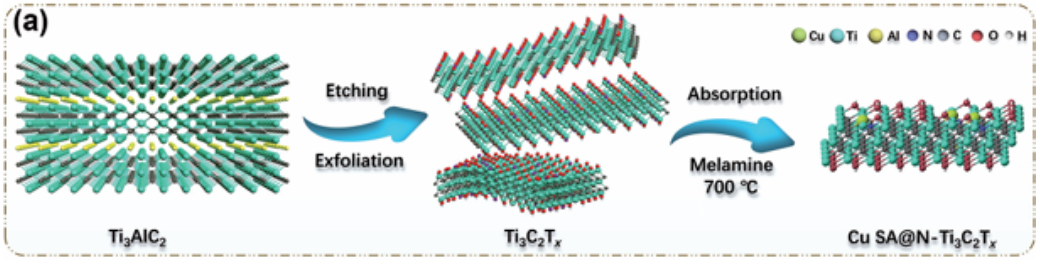

Figure 5. Interfacial charge transfer mechanism

3.3. Synergistic mechanisms of MXene quantum dots

The synergistic interplay among light absorption, charge transport, and surface reactions determines the enhanced photocatalytic performance of MQDs. Furthermore, different modification strategies optimize photogenerated carrier generation, interfacial transport, and CO_2 activation, thus enabling continuous regulation from light harvesting to reaction intermediate conversion.

For light absorption and charge transport, N/S co-doping modulates the electronic structure of MQDs and extends the visible-light response range, whereas heterostructure construction promotes carrier separation through interfacial band alignment, improving electron migration toward reaction sites. During the surface reaction process, –O terminal groups, defect sites, and Cu single-atom sites collectively provide CO_2 adsorption and activation centers, facilitating CO_2 molecular bending and electron injection, lowering the energy barrier of the initial reduction step. Meanwhile, appropriate regulation of intermediate adsorption strength aids in stabilizing key intermediates such as *CO and *CHO, driving the reaction along the stepwise hydrogenation pathway toward methanol generation. Under this mechanistic framework, the N, S-Cu/MQDs/g-C_3N_4 system achieves synergistic effects through "enhanced light absorption-optimized charge separation-regulated surface reaction sites," concentrating the electron flow to predominantly advance along the CO_2→*CO→*CHO→CH_3OH pathway during continuous charge transfer.

4. Structural evolution and photocatalytic performance of modified quantum dots

4.1. Structural engineering and photoelectronic response properties

Heteroatom doping, heterojunction construction, and single-atom modification can synergistically modulate the electronic structure and optoelectronic properties of MQDs, with their effects mainly on interfacial electronic regulation, band optimization, and carrier dynamics. Meanwhile, structural characterization reveals that modified MQDs generally maintain nanoscale morphological stability, with surface functionalization predominantly influencing the local electronic environment without greatly compromising structural integrity [6]. Moreover, at the interfacial electronic structure level, heterojunction hybridization induces charge redistribution at the interface, as shown by systematic shifts in XPS binding energies, consistent with the built-in electric field-driven mechanism of S-scheme heterojunctions. In the N,S-Cu/MQDs/g-C_3N_4 system, the Ti 2p binding energy shows an overall shift of approximately 0.4 eV [10].

DOI: 10.54254/2755-2721/2026.36617

At the optical response level, N/S co-doping introduces localized energy levels and modulates the band structure via N 2p–Ti 3d hybridization, extending the absorption edge into the visible-light region beyond 550 nm, extending the effective spectral range for carrier generation. At the carrier dynamics level, enhanced photocurrent response and prolonged time-resolved fluorescence decay appear concurrently, indicating improved interfacial charge separation efficiency and suppressed nonradiative recombination processes, with the average carrier lifetime extended to the nanosecond scale.

4.2. MXene interface-driven CO_2 conversion behavior

The surface terminal groups of MXene quantum dots and metal single-atom sites jointly construct CO_2 adsorption and activation interfaces. Under low partial pressure conditions, oxygen-containing functional groups such as –O and metal active centers can enhance CO_2 surface enrichment and facilitate the transition from physisorption to chemisorption. Existing studies reveal that modified MQDs demonstrate CO_2 adsorption capacities of 1.1–1.2 mmol·g^{-1} under simulated air conditions, representing a 2–3-fold enhancement over unmodified systems (~0.4 mmol·g^{-1}) [6, 16].

Building on this interfacial enrichment, the adsorption process can further induce CO_2 molecular bending, promoting electron transfer to antibonding orbitals and also reducing the activation barrier. Operando DRIFTS observations have detected key intermediate signals corresponding to COOH (1695 cm^{-1}) and OCH_3 (1155 cm^{-1}), showing that the CO_2 reduction involves adsorption, activation, carboxyl formation, and sequential hydrogenation, with interfacial sites governing intermediate stabilization and charge transfer. With interfacial enrichment and pathway regulation, modified MQD systems achieve a CO_2 conversion rate of 58.6 $\mu mol \cdot g^{-1} \cdot h^{-1}$, far higher than unmodified systems (12.3 $\mu mol \cdot g^{-1} \cdot h^{-1}$), as shown in Figure 6.

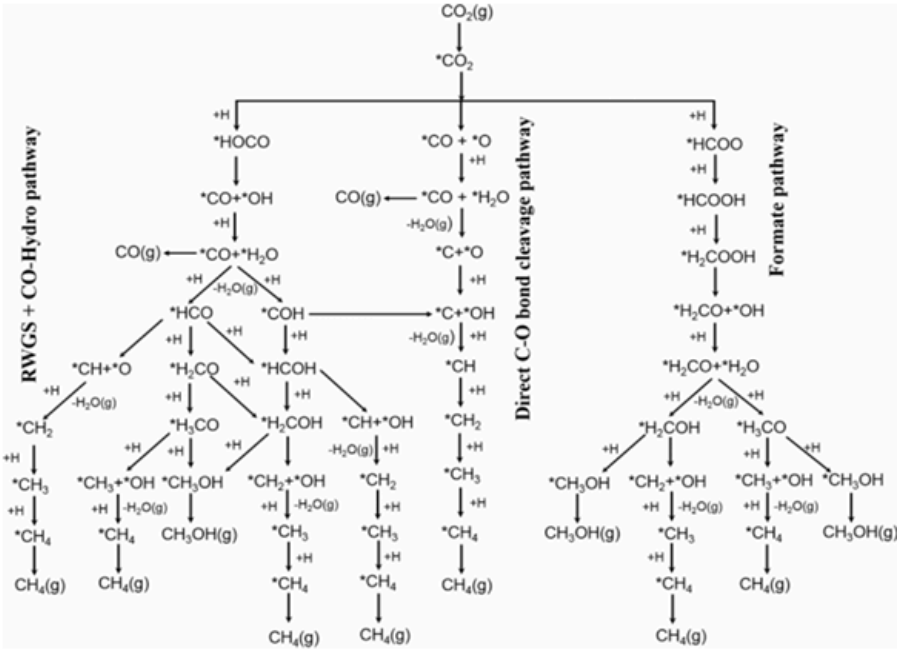

Figure 6. CO_2 adsorption and conversion performance of MQD-based catalysts

DOI: 10.54254/2755-2721/2026.36617

4.3. Effects of product selectivity and reaction conditions

Regarding product selectivity, Cu single-atom modification suppresses hydrogen evolution during CO_2 reduction and promotes carbon product formation. Prior studies have shown that the methanol electron selectivity in Cu single-atom/MXene composite systems typically ranges from 70% to 90% [19, 20]. At a Cu loading of 1.5 wt%, methanol dominates the liquid-phase products, while no C_2+ alcohols or hydrocarbons are detected by GC-FID and HPLC-MS. The methanol production rate reaches 36.8 $\mu mol \cdot g^{-1} \cdot h^{-1}$ with an electron selectivity of 85.7%, whereas the CO selectivity is only 9.1%, indicating that Cu sites favor the conversion of CO_2 toward the methanol pathway.

In terms of cycling stability, Cu-modified MQDs maintain 91.2% of their initial methanol yield after five photo-reaction/regeneration cycles, with no significant structural changes observed by XRD/XPS. Based on the stability of MXene materials, Cu/MXene photocatalytic systems typically retain 85-95% performance after 5-10 cycles. Meanwhile, reaction conditions affect CO_2 reduction performance. For example, increased light intensity enhances photogenerated carrier generation and promotes methanol production [8]. Furthermore, moderate water vapor levels (RH 10%-50%) can facilitate the CPET process, while excessive humidity inhibits reaction efficiency by competing for active sites [8, 21]. Beyond reaction environment factors, quantum dot size also modulates the band structure via quantum confinement effects. However, smaller MQDs can enhance the electronic reduction capability and CO_2 conversion driving force, whereas smaller sizes increase defects and carrier recombination, necessitating optimization of the balance between particle size and defect structure [14, 18].

5. CO_2 reduction mechanism of modified MXene quantum dots

5.1. Band regulation and interfacial charge reconstruction

In N-doped $Ti_3C_2T_x$, N 2p–Ti 3d orbital hybridization introduces localized electronic states near the Fermi level, reconstructing the band structure and enhancing visible-light response capability [18]. This type of hybridized state primarily modulates the electron occupancy distribution near the Fermi level, thereby altering the excitation behavior of the system. In MQD/g-C_3N_4 heterostructures, spontaneous formation of a built-in potential gradient occurs at the interface due to work function differences, driving electron migration from g-C_3N_4 toward the MQD side and achieving interfacial charge redistribution [10]. As illustrated in Figure 7, this architecture enables spatial electron-hole separation, suppresses interfacial recombination, and improves carrier utilization efficiency. Based on this foundation, band regulation and interfacial charge reconstruction jointly determine charge separation and electron distribution.

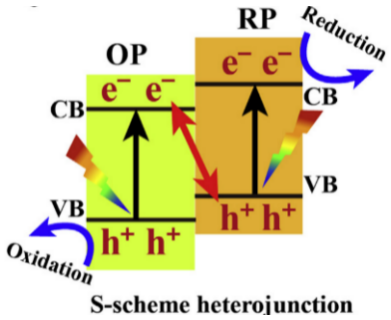

Figure 7. Photocatalytic mechanism of the S-scheme heterojunction

DOI: 10.54254/2755-2721/2026.36617

5.2. Surface site regulation and CO_2 activation mechanism

Theoretical calculations and spectroscopic studies have demonstrated that Cu single-atom sites can promote CO_2 activation through local electronic structure modulation. Existing investigations on Cu single-atom/MXene and Cu single-atom/carbon-based systems have shown that Cu sites can induce CO_2 configuration changes and modulate subsequent reduction reaction pathways [19, 20]. Based on these mechanistic principles, it is inferred that CO_2 adsorbed at Cu sites can undergo a transition from a linear configuration to a bent structure, accompanied by electron transfer that enhances C=O bond activation. This hypothesis is supported by the electron localization function (ELF) and Bader charge analyses of the N, S-Cu/MQDs/g-C_3N_4 system, which reveal that CO_2 adsorption reduces the ∠OCO angle from 180° to 137°, accompanied by a charge transfer of ~0.72 e^-. Further analysis indicates that neighboring Ti–O sites can stabilize adsorbed CO_2 through hydrogen bonding interactions, reducing the free energy barrier of the initial hydrogenation step ($*CO_2 + H^+ + e^- \rightarrow *COOH$) from 1.35 eV in the pristine MQD system to 0.48 eV. This energy barrier falls within the range of 0.4–0.8 eV reported for Cu-based catalytic systems, suggesting that Cu–Ti dual-site synergy may facilitate the initial CO_2 hydrogenation process [22].

5.3. Photogenerated carrier separation and recombination suppression

The modified MQD system boosts carrier separation and suppresses recombination. Femtosecond transient absorption spectroscopy reveals that pristine MQDs show rapid excited-state decay, mainly associated with carrier recombination. In contrast, the modified system exhibits a greatly extended lifetime and a fast initial decay component, suggesting enhanced interfacial charge transfer and reduced carrier recombination, as shown in Figure 8. Consequently, heterointerface coupling and Cu active sites promote electron migration to MQDs/Cu sites, while holes remain on g-C_3N_4, enabling spatial charge separation and sustained CO_2 reduction.

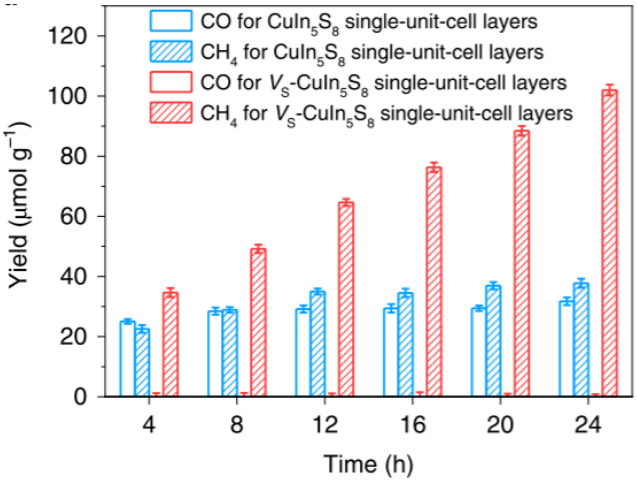

Figure 8. Comparison of femtosecond transient absorption spectra of MQDs before and after modification

5.4. Intermediate adsorption and product routes

Through CO adsorption strength regulation, reaction pathways are regulated. Accordingly, weak adsorption facilitates CO desorption, moderate adsorption supports CHO formation, while strong

DOI: 10.54254/2755-2721/2026.36617

adsorption hinders active-site turnover. As shown in Figure 9, CO adsorption on pristine MQDs is weak, with an adsorption energy of −0.11 eV, thus leading to rapid CO desorption and gaseous CO formation. After Cu introduction, the adsorption energy increases to −0.67 eV, enabling stable CO retention and further hydrogenation. Theoretical analysis suggests that the CO→CHO step exhibits a lower energy barrier than competing pathways (CO desorption and hydrogen evolution), indicating that Cu sites may regulate CO intermediate conversion toward methanol formation. Furthermore, the Cu/Ti interfacial synergy optimizes the adsorption behavior of oxygen-containing intermediates, reducing the energy requirement of the methanol formation pathway and thereby facilitating CO_2 conversion toward CH_3OH.

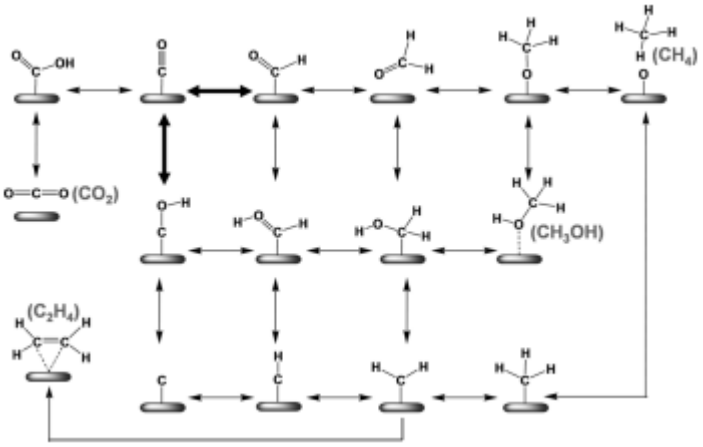

Figure 9. Gibbs free energy diagram for CO_2 reduction to CH_3OH

6. Conclusion

This paper reviews the research progress in multi-scale synergistic regulation of photocatalytic CO_2 conversion at atmospheric concentrations using MXene quantum dots. The analysis shows that band engineering, interfacial charge reconstruction, and surface site regulation synergistically optimize carrier separation and CO_2 adsorption/activation, enabling selective methanol formation through multi-electron transfer routes. By integrating S-scheme charge separation, Cu–Ti–O dual-site CO_2 activation, and intermediate adsorption tuning, the overall reaction efficiency is enhanced. However, the effects of atmospheric components such as O_2 and H_2O on active-site stability remain unclear; scalable fabrication of single-atom and quantum dot structures requires further improvement; and continuous-flow DAC system design under practical conditions remains insufficient. Future efforts should develop antioxidant and self-healing interfaces, establish green continuous synthesis routes, and construct photo–electro–flow coupled DAC systems to advance practical carbon conversion.

References

[1] International Energy Agency. (2024). CO_2 emissions in 2023. https://www.iea.org/reports/co2-emissions-in-2023
[2] Intergovernmental Panel on Climate Change. (2023). Climate change 2023: Synthesis report (H. Lee & J. Romero, Eds.). Contribution of Working Groups I, II and III to the Sixth Assessment Report of the Intergovernmental Panel on Climate Change. Cambridge University Press. https://doi.org/10.59327/IPCC/AR6-9789291691647
[3] Sanz-Pérez, E. S., Murdock, C. R., Didas, S. A., & Jones, C. W. (2016). Direct capture of CO_2 from ambient air. *Chemical Reviews, 116*(19), 11840-11876. https://doi.org/10.1021/acs.chemrev.6b00173
[4] Shi, X., et al. (2020). Sorbents for the direct capture of CO_2 from ambient air. *Angewandte Chemie International Edition, 59*(18), 6984–7006. https://doi.org/10.1002/anie.201906756

DOI: 10.54254/2755-2721/2026.36617

[5] Deutz, S., & Bardow, A. (2021). Life-cycle assessment of an industrial direct air capture process based on temperature–vacuum swing adsorption. *Nature Energy, 6*, 203–213. https://doi.org/10.1038/s41560-020-00771-9
[6] Alhabeb, M., et al. (2017). Guidelines for synthesis and processing of two-dimensional titanium carbide (Ti_3C_2Tx MXene). *Chemistry of Materials, 29*(18), 7633–7644. https://doi.org/10.1021/acs.chemmater.7b02847
[7] Shao, B., et al. (2020). Two-dimensional transition metal carbide and nitride (MXene) derived quantum dots (QDs): Synthesis, properties, applications and prospects. *Journal of Materials Chemistry A, 8*, 7508-7535.
[8] Chang, X., Wang, T., & Gong, J. (2016). CO_2 photo-reduction: Insights into CO_2 activation and reaction on surfaces of photocatalysts. *Energy & Environmental Science, 9*(7), 2177-2196.
[9] Li, X., Yu, J., Jaroniec, M., & Chen, X. (2019). Cocatalysts for selective photoreduction of CO_2 into solar fuels. *Chemical Reviews, 119*(6), 3962–4179. https://doi.org/10.1021/acs.chemrev.8b00400
[10] Xu, Q., Zhang, L., Cheng, B., Fan, J., & Yu, J. (2020). S-scheme heterojunction photocatalyst. *Chem, 6*(7), 1543–1559. https://doi.org/10.1016/j.chempr.2020.06.010
[11] Freund, H. J., & Roberts, M. W. (1996). Surface chemistry of carbon dioxide. *Surface Science Reports, 25*(8), 225–273. https://doi.org/10.1016/S0167-5729(96)00007-6
[12] Álvarez, A., Borges, M., Corral-Pérez, J. J., Olcina, J. G., Hu, L., Cornu, D., ... & Pérez-Ramírez, J. (2017). CO_2 activation over catalytic surfaces. *ChemPhysChem, 18*(22), 3135–3141. https://doi.org/10.1002/cphc.201700782
[13] Birdja, Y. Y., Pérez-Gallent, E., Figueiredo, M. C., Göttle, A. J., Calle-Vallejo, F., & Koper, M. T. M. (2019). Advances and challenges in understanding the electrocatalytic conversion of carbon dioxide to fuels. *Nature Energy, 4*, 732–745. https://doi.org/10.1038/s41560-019-0450-y
[14] Li, A., Zhu, W., Li, C., Wang, T., & Gong, J. (2019). Rational design of yolk–shell nanostructures for photocatalysis. *Chemical Society Reviews, 48*(7), 1874–1907. https://doi.org/10.1039/C8CS00711J
[15] Gao, G., O'Mullane, A. P., & Du, A. (2017). 2D MXenes: A new family of promising catalysts for the hydrogen evolution reaction. *ACS Catalysis, 7*(1), 494–500. https://doi.org/10.1021/acscatal.6b02754
[16] Zeng, Z., Yan, Y., Chen, J., Zan, P., Tian, Q., & Chen, P. (2019). Boosting the photocatalytic ability of Cu_2O nanowires for CO_2 conversion by MXene quantum dots. *Advanced Functional Materials, 29*(18), 1806500. https://doi.org/10.1002/adfm.202010720
[17] Zhu, T., Snaider, J. M., Yuan, L., & Huang, L. (2019). Ultrafast dynamic microscopy of carrier and exciton transport. *Annual Review of Physical Chemistry, 70*, 219–244. https://doi.org/10.1021/acs.chemrev.2c00243
[18] Zhang, Y., Xia, B., Ran, J., et al. (2020). Atomic-level reactive sites for semiconductor-based photocatalytic CO_2 reduction. *Advanced Energy Materials, 10*(9), 1903879. https://doi.org/10.1002/aenm.201903868
[19] Zhao, Q., Zhang, C., Hu, R., et al. (2021). Selective etching quaternary MAX phase toward single atom copper immobilized MXene (Ti3C2Cl x) for efficient CO_2 electroreduction to methanol. *ACS Nano, 15*(3), 4927-4936.
[20] LeMercier, T. M., Thangamuthu, M., Kohlrausch, E. C., et al. (2024). Synergy of nanocrystalline carbon nitride with Cu single atom catalyst leads to selective photocatalytic reduction of CO_2 to methanol. *Sustainable Energy & Fuels, 8*(8), 1691-1703.
[21] Kattel, S., Liu, P., & Chen, J. G. (2017). Tuning selectivity of CO_2 hydrogenation reactions at the metal/oxide interface. *Journal of the American Chemical Society, 139*(29), 9739–9754. https://doi.org/10.1021/jacs.7b05362
[22] Grabow, L. C., & Mavrikakis, M. (2011). Mechanism of methanol synthesis on Cu through CO_2 and CO hydrogenation. *ACS Catalysis, 1*(4), 365–384. https://doi.org/10.1021/cs200055d